Nature Environment and Pollution Technology
An International Quarterly Scientific Journal

p-ISSN: 0972-6268 e-ISSN: 2395-3454	Vol. 17	No. 4	pp. 1055-1064	2018

Original Research Paper | Open Access

Methylene Blue Adsorption on *Aloe vera* Rind Powder: Kinetics, Isotherm and Mechanisms

Megat Ahmad Kamal Megat Hanafiah*(**)†, Siti Zubaidah Mohd Jamaludin*, Khadijah Khalid* and Shariff Ibrahim***

*Faculty of Applied Sciences, Universiti Teknologi MARA, 26400, Jengka, Pahang, Malaysia
**Institute of Science (IOS), Universiti Teknologi MARA, 40450, Shah Alam, Selangor, Malaysia
***Faculty of Applied Sciences, Universiti Teknologi MARA, 40450, Shah Alam, Selangor, Malaysia
†Corresponding author: Megat Ahmad Kamal Megat Hanafiah

Nat. Env. & Poll. Tech.
Website: www.neptjournal.com

Received: 20-12-2017
Accepted: 20-02-2018

Key Words:
Aloe vera
Adsorption kinetics
Isotherms
Methylene blue

ABSTRACT

In this work, untreated rind of *Aloe vera* (URAV) was applied as an adsorbent for removing a cationic dye, methylene blue (MB) from aqueous solutions under batch experiments. Adsorption parameters such as pH, URAV dosage, contact time and MB concentration were varied to determine the efficacy of MB removal. MB was more favoured to be removed at pH > 3 and URAV showed a fast adsorption process as the time required to achieve equilibrium was 30 min. The maximum adsorption capacity recorded from the non-linear expression of Langmuir isotherm model was 356 mg/g at room temperature (300 K). Both, the pseudo-first-order and pseudo-second-order models, were appropriate to predict the MB adsorption kinetics. Among the plausible adsorption mechanisms detected from the Fourier transform infrared (FTIR) spectrometer and the pH studies were hydrogen bonding, n-Π and Π-Π interactions, and electrostatic attraction. Owing to the fast removal and high adsorption capacity of MB, URAV can be applied as an adsorbent for MB removal from wastewater.

INTRODUCTION

The rapid growth of human population and industrial activities have led to serious environmental problems, especially in developing countries (Han et al. 2017, De Gisi et al. 2016). Numerous types of pollutants are constantly released into water bodies, which can be harmful to aquatic life and humans. The release of dyes from textile industries, paper and pulp industries, tannery and pharmaceutical industries has been identified as one of the major sources of water pollution. Dyes contain different chemical compounds such as organics, acids and heavy metals. Upon release into the environment, dyes will degrade, and their breakdown products can be carcinogenic and mutagenic to life forms (Zaharia et al. 2009). Methylene blue (MB) with molecular formula $C_{16}H_{18}N_3SCl$ (Fig. 1) is an example of synthetic cationic dye commonly used in medicine for staining of bacteria and parasites (Heiner Shirmer et al. 2011), as a redox indicator, and for colouring nylon, silk and wool.

When MB enters the water bodies, it can retard photosynthesis, slow down the growth of aquatic biota by reducing sunlight intensity, reduce the oxygen content, and decrease the recreation value of stream. If consumed by humans, MB can cause serious health problems such as nausea, improper breathing and increased heart rate, vomiting, methaemoglobinaemia (Mall et al. 2005), mental confusion, and necrosis (Hameed & Ahmad 2009). Therefore, MB must be carefully removed from industrial wastewaters and conventional treatment methods usually involve coagulation, flocculation, oxidation, electrochemical and membrane filtration. However, some of these methods have major drawbacks such as costly, not feasible to treat a large volume of wastewater, requires a long treatment time, and may create secondary pollution.

A much simpler and cost-effective method to remove MB can be achieved by using adsorption technique and nowadays, the focus of selection of adsorbents has shifted to the use of lignocellulosic wastes (LWs) instead of activated carbons. Leaves, stems, barks, seeds, and roots are examples of LWs which are highly abundant, low cost and capable of removing MB from aqueous solutions at a faster rate. Among them are carrot leaf powder (Kushwaha et al. 2014), *Eichhornia crassipes* root and stem (Wanyonyi et al. 2013), Cengal (*Neobalanocarpus hepmii*) bark and red chili (*Capsicum annum*) seed (Kristanti et al. 2016). However, the amount of MB that can be adsorbed by LWs remains a major challenge as many articles reported low adsorption capacities (< 100 mg/g) when LWs were used as adsorbents. LWs also have been reported to have a low surface area which poses a challenge in pollutant adsorption efficiency

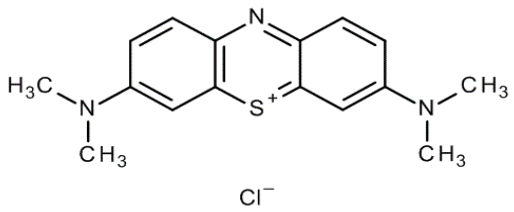

Fig. 1: Chemical structure of MB.

(Tran et al. 2016). For that reason, LWs are chemically or physically treated for introducing new functional groups or to increase the number of pores, which can improve adsorbent performance. However, the major drawbacks of chemically and physically treated LWs include (i) time consuming as a series of reactions are involved, (ii) high cost due to the consumption of expensive chemicals and energy, (iii) enhanced adsorption capacity cannot be guaranteed, and (iv) generation of toxic wastes during pre-treatment, which leads to a secondary pollution problem. Therefore, application of untreated LWs as adsorbents is still practiced in wastewater treatment, but a careful investigation on the chemical properties of LWs is required before they can be applied as adsorbents. Unlike activated carbons which have high surface area, untreated LWs lack porosity (Hanafiah et al. 2012, Khalir et al. 2011) and adsorption of pollutants mainly occurs at the external surface and not by pore filling mechanism. Therefore, identifying the types of functional groups present in LWs is a critical factor in determining an adsorbent efficiency and in understanding the mechanisms of adsorption.

Alkoxide, carboxylate, amino, and thiol are among important functional groups that provide adsorption sites for the attachment of cationic pollutants such as heavy metal ions and cationic dyes. *Aloe barbadensis* or *Aloe vera* (AV), a by-product of agricultural industry is known to contain complex chemical compounds which include amino acids, lignin, anthraquinones, minerals such as potassium, sodium, calcium and magnesium, proteins, enzymes, polysaccharides, lipids (waxes and sterols), and flavonoids (Baruah et al. 2016). AV shows numerous activities such as antioxidant, antimicrobial, antiallergic, antidiabetic, anticancer, antiulcer and anti-inflammatory; therefore, AV is considered as a very useful plant in food, cosmetic and pharmaceutical industries (Sanchez-Machado et al. 2017). The most important part of AV for industries is the clear pulp (jelly layer) while the thick green rind is often discarded (Liu et al. 2013). Due to the presence of numerous compounds found in AV, it is therefore important to evaluate its potential as an adsorbent for removing MB. A literature search has been conducted and to date, there has been no report on the application of AV rind powder to adsorb MB from aqueous solutions. In this work, the behaviour of MB adsorption onto AV rind powder (a by-product of LW), which includes effects of pH, dosage, rate of adsorption and adsorption isotherm were evaluated. The adsorption performance of AV based on maximum adsorption capacity would be compared with other reported LWs. The plausible mechanisms of MB adsorption were also proposed.

MATERIALS AND METHODS

Material: Fresh *Aloe vera* L. (*Aloe barbadensis* Mill.) leaves were obtained from a local farm in Masai, Malaysia. The leaves were cut and washed with deionized water to eliminate dust particles. The inner gel or fleshy part and yellowish sap of AV were carefully removed to ensure that only the green rind was left and used in adsorption experiments. The cleaned rind was dried in an oven at 353 K overnight, crushed using a laboratory mill and sieved to obtain the average adsorbent size of < 180 μm. No chemical treatment was performed on AV rind powder to avoid a major loss of chemical constituents due to leaching process during treatment and hence, the weight of adsorbent would also be greatly reduced. The untreated rind powder of AV was designated URAV and used throughout the experiments.

Characterization of URAV: URAV was characterized by using an Attenuated Total Reflectance-Fourier Transform Infrared (ATR-FTIR) spectrometer (Perkin Elmer, Spectrum 100, USA) and pH of zero-point charge (pH_{zpc}). Degradation profile of URAV based on temperature was performed by using a thermogravimetric analyser (TGA, Pyris 1, Perkin Elmer, USA). Approximately 5 mg of URAV was placed onto a platinum crucible and heated at 20°C/min under N_2 flow with the temperature ranging from 25°C to 700°C. In the ATR-FTIR analysis, URAV was subjected to 32 scans in a 4 cm^{-1} resolution. In the pH_{zpc} determination, a series of 50 mL (0.01 M) NaCl (background electrolyte) solutions were prepared in Erlenmeyer flasks and the pH was adjusted from 2 to 10 by addition of 0.10 M HCl or NaOH solutions. Then, 0.10 g URAV was added to each flask, sealed, and shaken in a water bath shaker (temperature of 300 K) for 24 h. URAV was filtered and the final pH of solutions in each flask was measured using a pH meter.

Batch adsorption experiments: MB was purchased from Merck, Germany, and a 1000 mg/L stock solution was prepared using deionized water. Working concentration solutions of MB were prepared by appropriate dilution. All adsorption experiments were conducted at room temperature of 300 K and stirring rate of 120 rpm. The effect of MB on solution pH was investigated at different initial pH values (3-10). Each flask was filled with 100 mL (20 mg/L) MB solution and the amount of UAV added was 0.02 g. The pH

of MB solution was adjusted by adding 0.10 M HCl or NaOH solution. Effect of URAV dosage was performed by varying the weight of URAV (0.02-0.10 g) in 100 mL MB solutions, while the pH and concentration of MB were kept constant at 7 and 20 mg/L, respectively. Adsorption kinetic studies were conducted using three different concentrations of MB (10, 20 and 30 mg/L) and URAV dosage of 0.02 g in 50 mL solutions. Adsorption isotherm experiments were carried out for MB concentrations of 10 to 100 mg/L at a constant temperature of 300 K and URAV dosage of 0.02 g. After predetermined time intervals, MB solutions were filtered and the remaining concentration of MB in the filtrates was measured using a UV-Visible spectrophotometer (UV 1800, Shimadzu, Japan) at λ_{max} = 665 nm. This maximum absorbance wavelength did not change with changes in pH of the solution from 2 to 10. All adsorption experiments were performed in duplicates and results were presented as mean. The relative standard deviation for all adsorption experiments was < 4%. The amount of MB adsorbed (q) and the percentage of removal were calculated using Eqs. 1 and 2, respectively:

$$q = (C_o - C_t).V/m \quad ...(1)$$

$$\% \text{ removal} = (C_o - C_t).100/C_o \quad ...(2)$$

Where, C_o and C_t are the initial and final MB concentrations (mg/L) at time t (min), respectively; m is the weight of URAV (g) and V is the MB volume (mL). The trial-and-error nonlinear methods were performed by using the Solver add-in (Microsoft Excel) to calculate the parameters of adsorption kinetics and adsorption isotherm models. For determining the best fit model, the chi-squared and coefficient of determination formulas were used, given by equations 3 and 4, respectively:

$$\chi^2 = \sum \frac{(q_{e,exp} - q_{e,cal})^2}{q_{e,cal}} \quad ...(3)$$

$$R^2 = 1 - \frac{\sum (q_{e,exp} - q_{e,cal})^2}{\sum (q_{e,exp} - q_{e,mean})^2}$$

$$= \frac{\sum (q_{e,cal} - q_{e,mean})^2}{\sum (q_{e,cal} - q_{e,mean})^2 + \sum (q_{e,cal} - q_{e,exp})^2} \quad ...(4)$$

Where, $q_{e,exp}$ and $q_{e,cal}$ are the amount of MB adsorbed (mg/g) at equilibrium determined from equation 1 and the model after using the Solver add-in, respectively; and $q_{e,mean}$ (mg/g) is the mean of $q_{e,exp}$ values.

RESULTS AND DISCUSSION

Characterization of URAV: The FTIR spectrum (Fig. 2) shows the presence of complex compounds in URAV. The broad peak from 2600 to 3200 cm^{-1} represents the carboxylic acid (-COOH) group. Stretching of -O-H and -N-H bonds could be detected at 3200 - 3600 cm^{-1}. The asymmetric and symmetric stretching of -C-H bonds were represented by the peaks at 2918 and 2850 cm^{-1}, respectively. The weak peak at 1784 cm^{-1} indicated the presence of ester group (-COOR). The strong and broad peak at 1586 cm^{-1} suggested the bending vibration of C=C of the aromatic ring from lignin which overlapped with the carbonyl (C=O of carboxylic acid) and $-NH_2$ bending groups. The -OH bending of carboxylic acid, C-N stretching and C-O-C group could be assigned to the peaks at 1394, 1315 and 1003 cm^{-1}, respectively. A small peak at 903 cm^{-1} is attributed to the presence of β-glycosidic linkages between monosaccharides (Fiore et al. 2004). The peak at 812 cm^{-1} represents the C-H group of aromatic hydrogen. Based on the above identification of FTIR peaks, it can be concluded that URAV contains main functional groups such as hydroxyl, amino, carboxylic acid, ether and aromatic rings. These functional groups are commonly found in plants as polysaccharides (mainly cellulose), lignin, proteins, chlorophyll, uronic acids and anthraquinones (Baruah et al. 2016, Flores-López et al. 2016).

URAV after being adsorbed by MB showed some distinctive changes in intensity and wave number shift, thus could suggest the possible mechanisms involved during MB adsorption. For instance, the peak at 3534 cm^{-1} disappeared after adsorption, possibly due to the formation of hydrogen bonding between H atoms of amino and hydroxyl groups of URAV and N atoms of MB. Another type of hydrogen bonding was also possible in the MB-URAV adsorption system, involving hydroxyl groups of URAV and the aromatic rings of MB. This kind of interaction is known as Yoshida H-bonding and has been reported by Blackburn (2004) in the removal of Reactive Red 238. The decrease in intensity and upshift of the peak from 1585 to 1598 cm^{-1} could indicate the formation of Π-Π interaction between aromatic rings of MB and C=C of URAV, which is in good agreement with the observation of Tran et al. (2017). As URAV contains oxygen groups such as R-OH, RCOOR, and C-O-C, the n-Π interaction (known as electron donor-acceptor interaction) between lone pairs of oxygen (in URAV) and the aromatic rings of MB could not be ruled out. In this type of interaction, the oxygen groups of URAV act as the electron donor, while the aromatic rings of MB represent the electron acceptors. Meanwhile, a much higher intensity of the peak at 1018 cm^{-1} indicated the presence of -S- group of MB, thus confirming the attachment of MB group on URAV surface. In summary, a combination of electrostatic forces, weak van der Waals interaction and hydrogen bonding was responsible for the MB adsorption onto URAV. However, determining the dominant mechanism(s) in MB adsorption requires a further extensive research.

Fig. 3 shows the degradation profile of URAV based on the TGA analysis. The TGA and DTG curves observed between 40°C and 190°C represent the vaporization of water absorbed in URAV. The weight loss recorded at 200°C to 280°C was due to hemicellulose decomposition, while cellulose degraded at a higher temperature (300-380°C). Lignin has a high thermal stability (Postai et al. 2016) and it has a wider range of decomposition temperature (200-700°C). The major weight loss of 35%, which occurred at 410°C, was attributed to lignin decomposition. The amount of solid residue remaining at 700°C was about 23 wt %. The different temperature of degradation observed in Fig. 3 is related to the differences in polymer structures (length, cross-linkage and chemical nature of the three main components present in URAV). Hemicellulose consists of saccharides (glucose, xylose, mannose and galactose) (Perez et al. 2002), it appears random with rich in branches, has an amorphous structure and is easy to decompose at low temperatures. Cellulose, on the other hand, is a linear polysaccharide, exists as long thread like fibres and has a strong intermolecular and intramolecular hydrogen bonding. Therefore, cellulose degrades at a temperature higher than hemicellulose. Lignin has many aromatic rings with various branches (high degree of cross-linking between phenylpropane units) (Ramiah 1970), and it acts as a cementing material in plants and provides mechanical strength. These factors cause lignin to be more thermally stable than hemicellulose and cellulose.

Different functional groups such as hydroxyl, amino, ether and carboxylic acid as detected from the FTIR spectrum (Fig. 2), indicating the base and acidic groups were present in URAV. Therefore, the surface of URAV carried positive and negative charges and these groups have a major influence on the behaviour of MB uptake. The pH at which the surface charge of an adsorbent equals zero is known as pH_{zpc} (also known as equal densities of positive and negative charges). The plot is shown in Fig. 4 and the pH_{zpc} value was 6.20. At pH < pH_{zpc}, URAV would carry more positive charges than negative charges and vice versa. As MB carries positive charge, adsorption of MB would be favourable at pH > pH_{zpc}.

Effect of pH on MB adsorption: It is well known that the pH of a solution can affect the surface charge of an adsorbent, the chemical form of an adsorbate and the type of interaction (complexation or electrostatic attraction) between adsorbate and adsorbent. The effect of pH on MB adsorption by URAV is shown in Fig. 5. The amount of MB adsorbed was significantly affected at pH < 4 and a small variation in q_e (mg/g) was observed from pH 4 to 10. At pH 3, the acidic groups in URAV such as -COOH and -OH were being protonated, causing a greater repulsion force between MB and these positively charged groups. Hence, the amount of MB adsorbed was very low. As pH increased to 4, the carboxylic acid (-COOH) would dissociate to produce carboxylate ($-COO^-$), which resulted in binding of MB via electrostatic attraction. This explains why adsorption of MB on URAV was possible at pH < pH_{zpc}. Manna et al. (2017) reported a similar finding in the removal of MB by neem oil phenolic resin. A further increase in pH, especially at pH > pH_{zpc}, would expose more negative charges on URAV surface which favoured a higher uptake of MB. However, electrostatic attraction alone was not the only mechanism

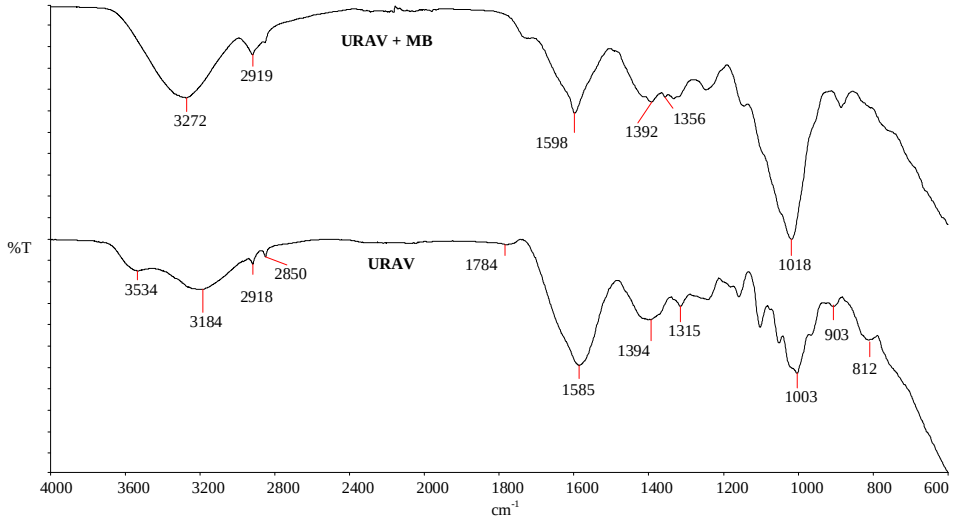

Fig. 2: FTIR spectra of URAV before and after contact with MB.

involved as URAV could attract MB via hydrogen bonding, n-Π and Π-Π interactions as revealed by FTIR spectra (Fig. 2).

Effect of URAV dosage: In a wastewater treatment facility, finding the optimum amount of adsorbent for removal of known concentration and volume of a pollutant is crucial as this practice can save the cost of operation. Besides, adsorbent dosage also determines the availability and accessibility of adsorption sites. Therefore, the effect of URAV dosage on MB adsorption was carried out and the results are shown in Fig. 6. The plots showed opposite relationship between the amount of MB adsorbed (q_e, mg/g) and the percentage removed. The percentage of MB removal was increased by only 8 % as the URAV dosage was increased from 0.02 to 1.0 g. More adsorption sites were available for MB when URAV dosage was increased, resulting in a higher percentage of MB removed. The decline in the amount of MB adsorbed, however, was associated with the mass balance equation (Eq. 1). This equation provides two major informations which are the number of available adsorption sites and the number of deactivated adsorption sites at the high adsorbent dosage (Marzbali et al. 2017). When the URAV dosage was increased, the ratio of adsorption sites to the number of MB molecules would decrease, leaving more number of unadsorbed sites and hence reduced the q_e (mg/g) values.

Collision among adsorbent particles also became more pronounced at a higher dosage, resulting in aggregation of particles, and would lead to the occurrence of deactivated adsorption sites. In addition, the weak bonds (physical adsorption) that hold MB molecules to URAV could be easily broken when the adsorbent particles collided, hence MB molecules were transferred back to the aqueous phase. Based on the dosage trend, a lower amount of URAV (0.02 g) was preferred for subsequent adsorption experiments as the five-fold increment in URAV dosage only resulted in a very small change in the percentage of MB removed but a large difference in q_e (mg/g).

Adsorption rate and kinetic models: The rate at which pollutants are removed from aqueous solutions is another crucial factor in the selection of suitable adsorbent for use in wastewater treatment facility. Depending on the concentration of MB, the time required for MB to achieve adsorption equilibrium has been reported by many studies to range from few minutes to few hours (Chen et al. 2017, Khalid & Hanafiah 2014). Fig. 7 shows the plots of the amount of MB

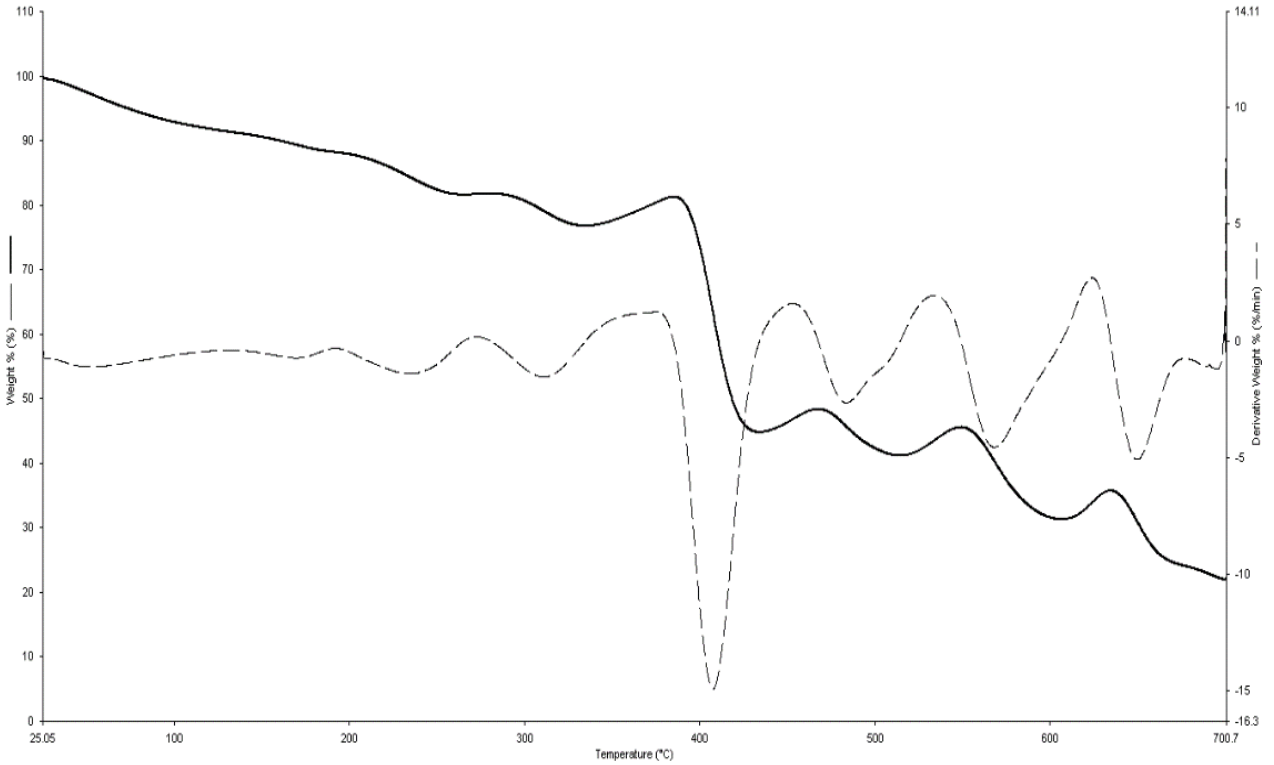

Fig. 3: The TGA and DTG curves of URAV.

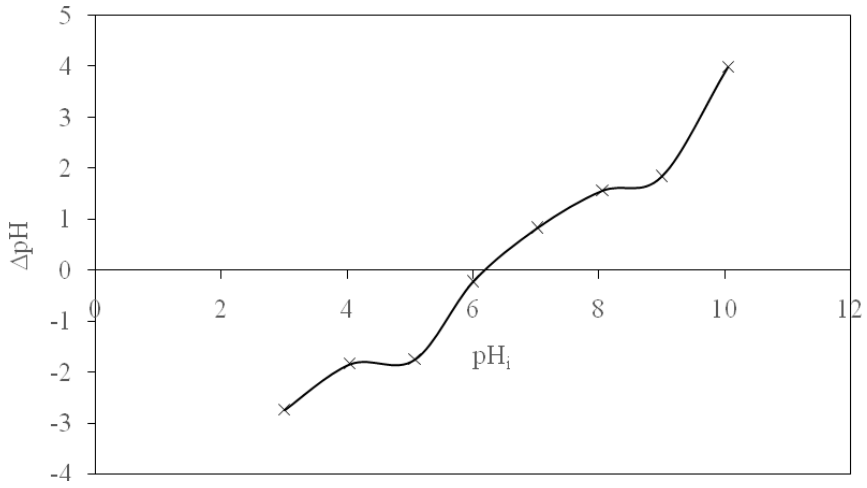

Fig. 4: pH_{zpc} plot of URAV.

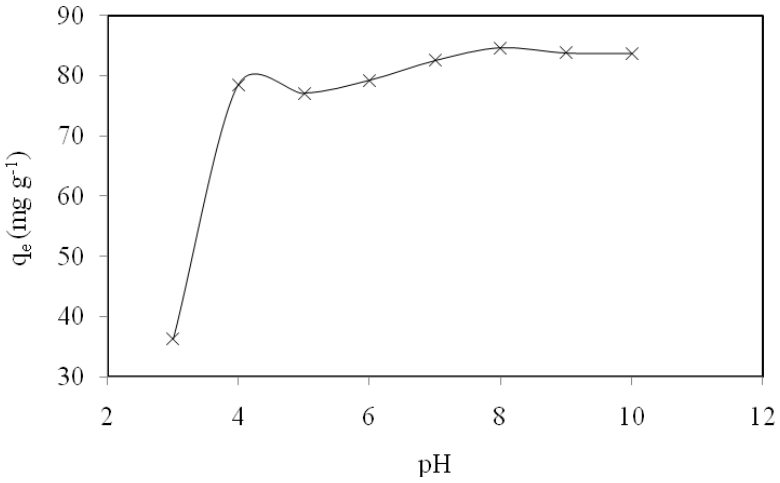

Fig. 5: Effect of pH on MB adsorption.

adsorbed (mg/g) versus time (min) at three different concentrations. URAV demonstrated a favourable property of an adsorbent as a high amount of MB could be adsorbed within the first 10 min. After 10 min of contact time, there was a very small increment in the amount of MB adsorbed and equilibrium time was recorded after 30 min. The initial rapid phase of adsorption was due to the presence of a high number of uncovered adsorption sites and strong attractive forces. As these sites were adsorbed, the rate of adsorption slowed down. It can be noticed that the amount of MB adsorbed also increased with increasing concentration, which was due to higher driving force at higher MB concentrations and capable of overcoming the mass transfer resistance between URAV and liquid phase.

The data from this effect of concentration and contact time were further explored to determine the order of adsorption kinetics using the nonlinear pseudo-first-order (Lagergren 1898) and pseudo-second-order (Ho & McKay, 1998) models given by equations (5) and (6), respectively:

$$q_t = q_e(1 - e^{k_1 t}) \quad ...(5)$$

$$q_t = q_e^2 k_2 t/(1 + k_2 q_e t) \quad ...(6)$$

Where, q_t, k_1 and k_2 represent the amount of MB adsorbed (mg/g) at time t (min), the pseudo-first-order constant (min^{-1}) and pseudo-second-order rate constant (g.mg^{-1}.min^{-1}), respectively. The pseudo-first-order and pseudo-second-order parameters, R^2 and X^2 obtained are summarized in Table 1. The

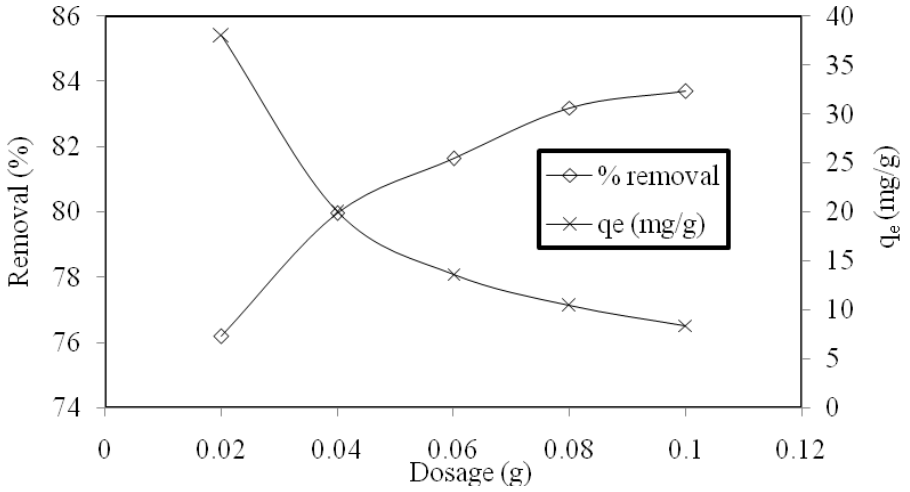

Fig. 6: Effect of URAV dosage on uptake of MB.

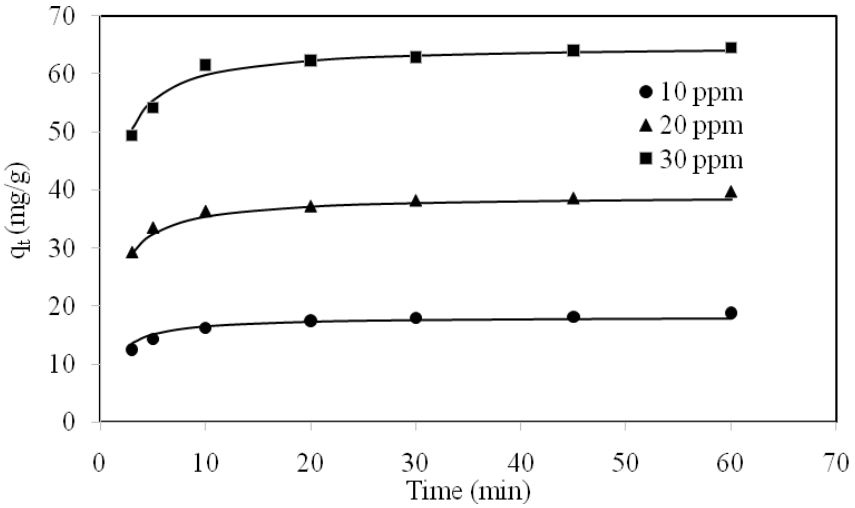

Fig. 7: Effect of concentration and contact time on MB adsorption.

k_1 values obtained were found to increase from 0.217 to 0.348 min^{-1} with increasing MB concentrations. Both kinetic models showed the calculated amounts of MB adsorbed at equilibrium are close to the experimental values, with R^2 values of the pseudo-first-order closer to unity. The lowest k_2 value was recorded at 30 mg/L MB, which suggested the longer time required to reach equilibrium, consistent with the results of most theoretical interpretations (Plazinski et al. 2009). A closer look at the X^2 values indicated that MB adsorption was better modelled by the pseudo-second-order model. It is important to note that both the kinetic models are a representation of surface reaction-controlled kinetics and they do not present a defined adsorption mechanism (Tan & Hameed 2017).

Adsorption isotherm: Adsorption isotherm is a study on the equilibrium relationship between the number of adsorbates adsorbed on the surface of an adsorbent and adsorbates remained unadsorbed in the solution. This study also provides a useful information on the possible adsorption mechanism such as the orientation of molecules adsorbed on the surface of an adsorbent. According to Giles et al. (1974), isotherms for organic solutes adsorption can be classified into four main classes (L, H, S and C curves) based on the slope of the initial portion of the curve, and the sub-groups (1 to 4) of each class can be described based on the shape of the upper part of the curve. As can be seen in Fig. 8, the isotherm curve is sigmoidal and has a point of inflection, which is a typical S3-type isotherm curve. Miraboutalebi et

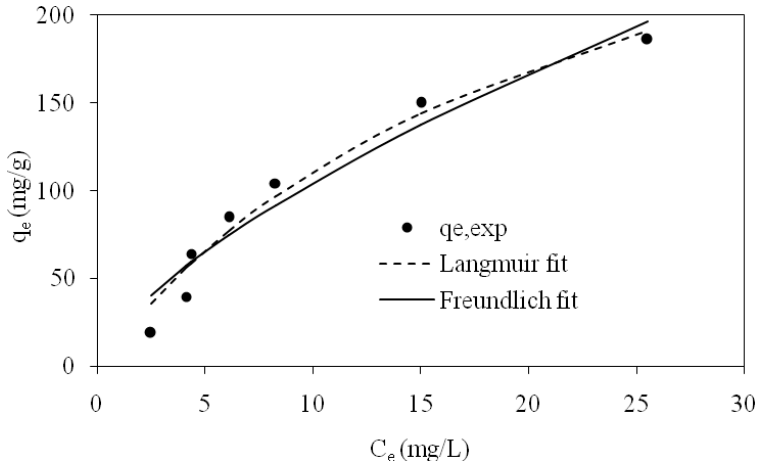

Fig. 8: Langmuir and Freundlich isotherm plots of MB adsorption.

Table 1: Pseudo-first-order and pseudo-second-order kinetics parameters calculated for MB adsorption on URAV.

MB mg/L	$q_{e,exp}$ mg/g	Pseudo-first-order $q_{e,cal}$	k_1	R^2	X^2	Pseudo-second-order $q_{e,cal}$	k_2	R^2	X^2
10	18.86	18.19	0.217	0.988	2.15	18.69	0.052	0.902	0.202
20	39.74	39.00	0.338	0.999	0.12	39.44	0.026	0.943	0.077
30	64.56	63.54	0.348	0.999	0.43	65.00	0.018	0.967	0.116

Table 2: Corresponding isotherm parameters of MB adsorption deduced from the Langmuir and Freundlich models.

Isotherm models	Value
Langmuir	
Q^o_{max}	356.0
K_L	0.045
R^2	0.964
X^2	15.01
Freundlich	
K_F	21.89
n	0.68
R^2	0.937
X^2	22.16

al. (2017) and Dotto et al. (2015) also reported a similar shape of the isotherm in the MB adsorption on maize silk powder and raw chitin, respectively. The low slope of the initial part of this curve represents a low amount of MB uptake at low initial MB concentrations, but MB would be easier to get adsorbed at higher concentrations. This isotherm suggests a side-by-side association between MB molecules, also called a "co-operative adsorption" (Giles et al. 1960).

The adsorption isotherm data obtained were further analysed by using the Langmuir (Langmuir 1918) and Freundlich models (Eqs. 7 & 8, respectively). A non-linear optimization technique is useful in minimizing error functions and therefore, it was applied to determine the adsorption parameters from these models.

$$q_e = \frac{Q^o_{max} K_L C_e}{(1 + K_L C_e)} \quad ...(7)$$

$$q_e = K_F C_e^n \quad ...(8)$$

Where, Q^o_{max} is maximum adsorption capacity (mg/g), K_L is the Langmuir constant (L/mg), K_F is the Freundlich constant [(mg/g)/(mg/L)^n], and n represents the adsorption intensity. The corresponding adsorption isotherm parameters are presented in Table 2.

Adsorption of MB on URAV can be concluded to follow the Langmuir isotherm model as this model recorded a higher non-linear regression (R^2) value and a lower value of X^2 compared to the Freundlich model. The maximum adsorption capacity was 356 mg/g and MB adsorption was favourable as the n value determined from the Freundlich model was < 1. As given in Table 3, URAV recorded a higher maximum adsorption capacity than the other reported LWs and activated carbons derived from corncob and *Cocos nucifera* L. Therefore, URAV has a good potential application to replace activated carbons in the treatment of wastewater containing MB.

Table 3: Comparison of URAV adsorption capacity with other reported adsorbents from LWs and activated carbons.

Types of LWs	q_{max} (mg/g)	pH	Temperature (K)	Equilibrium time (min)	Reference
URAV	356.0	8	300	30	This study
Karanj activated carbon	239.4	7	303	1440	Islam et al. (2017)
Citrus limetta peel waste	227.3	9	298	180	Shakoor & Nasar (2015)
Waste tea	212.8	6	298	120	Zhou et al. (2016)
Maize silk powder	234.1	12	298	80	Miraboutalebi et al. (2017)
Aleurites moluccana seeds	178.0	6	298	160	Postai et al. (2016)
Palm oil mill effluent	170.0	7.4	*NA*	1500	Zaini et al. (2016)
Oxidized weed char	161.9	7.4	323	480	Güzel et al. (2017)
Cauliflower leaf powder	149.2	9	303	100	Ansari et al. (2016)
Platanus orientalis leaf powder	114.9	12	333	70	Peydayesh & Rahbar Kelsihami (2015)
Ashoka leaf powder	90.9	6	303	50	Gupta et al. (2012)
Corncob activated carbon	82.7	7	303	100	Tharaneedhar et al. (2017)
Solanum tuberosum leaf powder	52.6	7	303	30	Gupta et al. (2016)
Aegle marmelos leaf powder	19.9	6.7	303	10	Baruah et al. (2017)
Cocos nucifera L. activated carbon	20.62	*NA*	323	*NA*	Sharma et al. (2010)

NA – not avaliable

CONCLUSION

This work revealed the potential application of URAV as an adsorbent for MB removal due to its high adsorption capacity (356 mg/g) and rapid uptake. The presence of numerous functional groups, particularly the hydroxyl, carboxyl, ether, amino and aromatic rings in URAV resulted in different mechanisms of MB adsorption particularly via electrostatic attraction, hydrogen bonding, n-Π and Π-Π interactions. As the adsorption capacity of URAV was higher than activated carbons, which are rich in micropores, adsorption of MB on URAV can be concluded to take place at the external surface rather than by pore filling. URAV also demonstrated good applicability in removing MB over a wide pH range (4 to 10). The pseudo-second-order and Langmuir models best fitted the kinetics and equilibrium adsorption studies, respectively.

REFERENCES

Ansari, S.A., Khan, F. and Ahmad, A. 2016. Cauliflower leave, an agricultural waste biomass adsorbent, and its application for the removal of MB dye from aqueous solution: Equilibrium, kinetics, and thermodynamic studies. Int. J. Anal. Chem., 216: Article ID 8252354, 10 pages

Baruah, A., Bordoloi, M. and Baruah, H.P.D. 2016. *Aloe vera*: a multipurpose industrial crop. Ind. Crop. Prod., 94: 951-963.

Baruah, A., Devi, A., Bhattacharyya, K.G. and Sarma, A. 2017. Developing a biosorbent from *Aegle marmelos* leaves for removal of methylene blue from water. Int. J. Environ. Sci. Technol., 14: 341-352.

Blackburn, R.S. 2004. Natural polysaccharides and their interactions with dye molecules: Applications in effluent treatment. Environ. Sci. Technol., 38: 4905-4909.

Chen, C., Fu, Y., Yu, L.L., Li, J. and Li, D.Q. 2017. Removal of methylene blue by seed-watermelon pulp-based low-cost adsorbent: Study of adsorption isotherms and kinetic models. J. Disper. Sci. Technol., 38: 1142-1146.

De Gisi, S., Lofrano, G., Grassi, M. and Notarnicola, M. 2016. Characteristics and adsorption capacities of low-cost sorbents for wastewater treatment: A review. Sustain. Mater. Technol., 9: 10-40.

Dotto, G.L., Santos, J.M.N., Rodrigues, I.L., Rosa, R., Pavan, F.A. and Lima, E.C. 2015. Adsorption of methylene blue by ultrasonic surface modified chitin. J. Colloid Interface Sci., 446: 133-140.

Fiore, V., Scalici, T., Nicoletti, F., Vitale, G., Prestipino, M. and Valenza, A. 2016. A new eco-friendly chemical treatment of natural fibres: Effect of sodium bicarbonate on properties of sisal fibre and its epoxy composites. Compos. Pt. B-Eng., 85: 150-160.

Flores-López, M.L., Romaní, A., Cerqueira, M.A., Rodríguez-García, R., de Rodríguez, D.J. and Vicente, A.A. 2016. Compositional features and bioactive properties of whole fraction from *Aloe vera* processing. Ind. Crop. Prod., 91: 179-185.

Giles, C.H., MacEwan, T.H., Nakhwa, S.N. and Smith, D. 1960. Studies in adsorption. Part XI. A system of classification of solution adsorption isotherms, and its use in diagnosis of adsorption mechanisms and in measurement of specific surface areas of solids. J. Chem. Soc., pp. 3973-3993.

Giles, C.H., Smith, D. and Huitson, A. 1974. A general treatment and classification of the solute adsorption isotherm. I. Theoretical. J. Colloid Interface Sci., 47: 755-765.

Gupta, N., Kushwaha, A.K. and Chattopadhyaya, M.C. 2012. Adsorption studies of cationic dyes onto Ashoka (*Saraca asoca*) leaf powder. J. Taiwan Inst. Chem. Eng., 43: 604-613.

Gupta, N., Kushwaha, A.K. and Chattopadhyaya, M.C. 2016. Application of potato (*Solanum tuberosum*) plant wastes for the removal of methylene blue and malachite green dye from aqueous solution. Arab. J. Chem., 9: S707-S716.

Güzel, F., Saygili, H., Saygili, G.A., Koyuncu, F. and Yilmaz, C. 2017. Optimal oxidation with nitric acid of biochar derived from pyrolysis of weeds and its application in removal of hazardous dye methylene blue from aqueous solution. J. Clean. Prod., 144: 260-265.

Hameed, B.H. and Ahmad, A.A. 2009. Batch adsorption of methylene blue from aqueous solution by garlic peel, an agricultural waste biomass. J. Hazard. Mater., 164: 870-875.

Han, S., Wang, T. and Li, B. 2017. Preparation of a hydroxyethyltitanium dioxide-carboxymethyl cellulose hydrogel cage and its effect on the removal of methylene blue. J. Appl. Polym. Sci., 134(23): 44925.

Hanafiah, M.A.K.M., Ngah, W.S.W., Zolkafly, S.H., Teong, L.C. and Majid, Z.A.A. 2012. Acid Blue 25 adsorption on base treated Shorea dasyphylla sawdust: Kinetic, isotherm, thermodynamic and spectroscopic analysis. J. Environ. Sci., 24: 261-268.

Heiner Schirmer, R., Adler, H., Pickhardt, M. and Mandelkow, E. 2011. Lest we forget you-methylene blue. Neurobiol. Aging, 32(12): 2325.e7-2325.e16.

Ho, Y.S. and McKay, G. 1998. A comparison of chemisorption kinetic models applied to pollutant removal on various sorbents. Process Saf. Environ. Protect., 76: 332-340.

Islam, M.A., Sabar, S., Benhouria, A., Khanday, W.A., Asif, M. and Hameed, B.H. 2017. Nanoporous activated carbon prepared from karanj (*Pongamia pinnata*) fruit hulls for methylene blue adsorption. J. Taiwan Inst. Chem. Eng., 74: 96-104.

Khalid, K. and Hanafiah, M.A.K.M. 2014. Kinetic and isotherm adsorption studies of methylene blue on sulfuric acid treated spent grated coconut (*Cocos nucifera*). Adv. Mater. Res., 970: 192-197.

Khalir, W.K.A.W., Hanafiah, M.A.K.M., Mat So'ad, S.Z. and Ngah, W.S.W. 2011. Adsorption behavior of Pb(II) onto xanthated rubber (*Hevea brasiliensis*) leaf powder. Polish J. Chem. Technol., 13: 82-88.

Kristanti, R.A., Kamisan, M.K.A. and Hadibarata, T. 2016. Treatability of methylene blue solution by adsorption process using *Neobalanocarpus hepmii* and *Capsicum annuum*. Water Air Soil Pollut., 227: 134.

Kushwaha, A.K., Gupta, N. and Chattopadhyaya, M.C. 2014. Removal of cationic methylene blue and malachite green dyes from aqueous solution by waste materials of *Daucus carota*. J. Saudi Chem. Soc., 18: 200-207.

Lagergren, S. 1898. About the theory of so-called adsorption of soluble substances. Kungliga Sven. Vetenskapsakad. Handl., 24(4): 1-39.

Langmuir, I. 1918. The adsorption of gases on plane surfaces of glass, mica, and platinum. J. Am. Chem. Soc., 40: 1361-1403.

Liu, P., Chen, D. and Shi, J. 2013. Chemical constituents, biological activity and agricultural cultivation of Aloe vera. Asian J. Chem., 25: 6477-6485.

Mall, D., Srivastava, V.C., Agarwal, N.K. and Mishra, I.M. 2005. Removal of congo red from aqueous solution by bagasse fly ash and activated carbon: Kinetic study and equilibrium isotherm analyses. Chemosphere, 61(4): 492-501.

Manna, S., Roy, D., Saha, P., Gopakumar, D. and Thomas, S. 2017. Rapid methylene blue adsorption using modified lignocellulosic materials. Process Saf. Environ. Protect., 107: 346-356.

Marzbali, M.H., Mir, A.A., Pazoki, M., Pourjamshidian, R. and Tabeshnia, M. 2017. Removal of direct yellow 12 from aqueous solution by adsorption onto spirulina algae as a high-efficiency adsorbent. J. Environ. Chem. Eng., 5: 1946-1956.

Miraboutalebi, S.M., Nikouzad, S.K., Peydayesh, M., Allahgholi, N., Vafajoo, L. and McKay, G. 2017. Methylene blue adsorption via maize silk powder: Kinetic, equilibrium, thermodynamic studies and residual error analysis. Process Saf. Environ. Protect., 106: 191-202.

Pérez, J., Munoz-Dorado, J., De la Rubia, T. and Martinez, J. 2002. Biodegradation and biological treatments of cellulose, hemicellulose and lignin: An overview. Int. Microbiol., 5(2): 53-63.

Peydayesh, M. and Rahbar-Kelishami, A. 2015. Adsorption of methylene blue onto *Platanus orientalis* leaf powder: Kinetic, equilibrium and thermodynamic studies. J. Ind. Eng. Chem., 21: 1014-1019.

Plazinski, W., Rudzinski, W. and Plazinska, A. 2009. Theoretical models of sorption kinetics including a surface reaction mechanism: A review. Adv. Colloid Interfac., 152: 2-13.

Postai, D.L., Demarchi, C.A., Zanatta, F., Melo, D.C.C. and Rodrigues, C.A. 2016. Adsorption of rhodamine B and methylene blue dyes using waste of seeds of *Aleurites moluccana*, a low-cost adsorbent. Alexandria Eng. J., 55: 1713-1723.

Ramiah, M. 1970. Thermogravimetric and differential thermal analysis of cellulose, hemicellulose, and lignin. J. Appl. Polym. Sci., 14(5): 1323-1337.

Sanchez-Machado, D.I., Lopez-Cervantes, J. and Sendon, R. 2017. *Aloe vera*: Ancient knowledge with new frontiers. Trends Food Sci. Technol., 61: 94-102.

Shakoor, S. and Nasar, A. 2016. Removal of methylene blue dye from artificially contaminated water using *Citrus limetta* peel waste as a very low-cost adsorbent. J. Taiwan Inst. Chem. Eng., 66: 154-163.

Sharma, Y.C., Sinha, A.S.K. and Upadhyay, S.N. 2010. Characterization and adsorption studies of *Cocos nucifera* L. activated carbon for the removal of methylene blue from aqueous solutions. J. Chem. Eng. Data, 55: 2662-2667.

Tan, K.L. and Hameed, B.H. 2017. Insight into the adsorption kinetics models for the removal of contaminants from aqueous solutions. J. Taiwan Inst. Chem. Eng., 74: 25-48.

Tharaneedhar, V., Kumar, P.S., Saravanan, A., Ravikumar, C. and Jaikumar, V. 2017. Prediction and interpretation of adsorption parameters for the sequestration of methylene blue dye from aqueous solution using microwave assisted corncob activated carbon. Sustain. Mater. Technol., 11: 1-11.

Tran, H.N., Wang, Y.F., You, S.J. and Chao, H.P. 2017. Insights into the mechanism of cationic dye adsorption on activated charcoal: The importance of Π-Π interactions. Process Saf. Environ. Protect., 107: 168-180.

Tran, H.N., You, S.J. and Chao, L.P. 2016. Thermodynamic parameters of cadmium adsorption onto orange peel calculated from various methods: A comparison study. J. Environ. Chem. Eng., 4: 2671-2682.

Wanyonyi, W.C., Onyari. J.M. and Shiundu, P.M. 2013. Adsorption of methylene blue dye from aqueous solutions using *Eichhornia crassipes*. Bull. Environ. Contam. Toxicol., 91: 362-366.

Zaharia, C., Suteu, D., Muresan, A., Muresan, R. and Popescu, A. 2009. Textile wastewater treatment by homogenous oxidation with hydrogen peroxide. Environ. Eng. Manage. J., 8(6): 1359-1369.

Zaini, M.A.A., Alias, N. and Che Yunus, M.A. 2016. Bio-polishing sludge adsorbents for dye removal. Polish J. Chem. Technol., 18(4): 15-21.

Zhou, R., Zhou, R., Zhang, X., Tu, S., Yin, Y., Yang, S. and Ye, L. 2016. An efficient bio-adsorbent for the removal of dye: Adsorption studies and cold atmospheric plasma regeneration. J. Taiwan Inst. Chem. Eng., 68: 372-378.